INORGANIC CHEMISTRY
FRONTIERS

RESEARCH ARTICLE

View Article Online
View Journal | View Issue

Cite this: *Inorg. Chem. Front.*, 2022, **9**, 1674

The effect of pore sizes on D_2/H_2 separation conducted by MOF-74 analogues†

Liqiong Li,[a,b] Chunqing Ji,[b,c] Wenjing Wang,[b] Fan Wu,[b] Yan-Xi Tan*[a,b] and Daqiang Yuan*[a,b]

Received 19th January 2022,
Accepted 20th February 2022

DOI: 10.1039/d2qi00156j

rsc.li/frontiers-inorganic

Four stable MOF-74 analogues, namely Ni_2(dobdc), Ni_2(dobpdc), Ni_2(olz) and Ni_2(dotpdc), possessing abundant open metal sites (OMSs) and honeycomb channels with pore sizes ranging from 1.0 to 2.6 nm, were used to research the effects of the pore size on D_2/H_2 separation from the hydrogen isotope mixture through dynamic column breakthrough experiments. With respect to consideration of the chemical affinity quantum sieving (CAQS) effect and the competitive adsorption between Ne and hydrogen isotope in (H_2/D_2/Ne: 1/1/98) and (H_2/D_2/Ne: 10/10/80) mixtures, the microporous Ni_2(dobdc) exhibits the longest breakthrough time periods of 240 and 36.4 min g^{-1}, respectively. In the (H_2/D_2: 50/50) mixture, mesoporous Ni_2(olz) exhibits the longest breakthrough time of 15.0 min g^{-1} owing to its more accessible OMSs and diffusion rate of hydrogen isotope being inclined to adsorb heavier D_2 rather than H_2. Hence, mesoporous MOFs with abundant OMSs may be ideal candidates for D_2/H_2 separation.

Introduction

With concerns over the development of sustainable energy sources, controlled fusion is seen as the ideal energy solution, and the International Thermonuclear Experimental Reactor (ITER) programme is researching and developing this technology. However, hydrogen isotope separation is one of the most critical technical issues in the ITER fuel cycle. To date, this technology has not been effectively overcome.[1–4] The extraction, separation, and purification of H_2 and D_2 are very difficult due to their almost identical sizes, shapes, and physicochemical properties. Traditional techniques, such as low-temperature distillation, thermal diffusion, centrifugation, laser separation, and chromatography, are energy-intensive, inefficient, and costly.[5–8] Based on the chemical affinity quantum sieving (CAQS) effect proposed by Prof. Oh, heavier D_2 preferentially adsorbed onto the strong active sites to achieve high D_2/H_2 separation.[9] Inspired by this, the assembling of strong active sites into porous frameworks will exhibit a highly efficient D_2/H_2 separation, and such physisorption has the advantages of low energy consumption, process simplicity, and low cost.[10,11]

Metal–organic frameworks (MOFs), as emerging materials with designable structures, large porosities, and abundant open metal sites (OMSs), are widely used in gas sorption and separation.[12–27] The use of MOFs as separation mixed-bed filters in flow separation systems for hydrogen isotope mixtures requires a very high selectivity for one of the components in the mixtures.[28] Therefore, MOFs with abundant OMSs as recognized strong active sites are ideal separating media for D_2/H_2 separation. For example, Cu(I)-MFU-4L with strong active Cu(I) sides demonstrated high D_2/H_2 selectivity at a very low temperature of 20 K, as measured by low-temperature thermal desorption spectroscopy.[29,30] In our previous studies, we investigated the D_2/H_2 separation properties of FYJ-Y11,[31] M-MOF-74,[32] and M_2(m-dobdc)[33] measured by the dynamic column breakthrough experiment, which is closer to simulating industrial separation processes. The famous MOF-74 series frameworks with high density of OMSs, particularly Co-MOF-74, exhibited satisfying D_2/H_2 separation performances. Although numerous mesoporous MOFs have been synthesized, chemists are more inclined to use microporous MOFs for D_2/H_2 separation because of their spatial confinement effects within the small pores. However, compared to microporous MOFs, mesoporous MOFs also have some advantages toward D_2/H_2 separation, including more accessible OMSs for preferential combination of heavier D_2 based on CAQS and large pores for increasing diffusion rate of the hydrogen isotope. No effort was focused on determining how the above two factors affected the sorption and separation of the hydrogen isotope, which inspired us to explore the D_2/H_2 separation using the mesoporous MOFs.

[a]*College of Chemistry, Fuzhou University, Fuzhou, 350108, China*
[b]*State Key Laboratory of Structural Chemistry, Fujian Institute of Research on the Structure of Matter, Chinese Academy of Sciences, Fuzhou, 350002 Fujian, China*
[c]*University of the Chinese Academy of Sciences, Beijing, 100049, China.*
E-mail: tyx@fjirsm.ac.cn, ydq@fjirsm.ac.cn

† Electronic supplementary information (ESI) available: Additional diagrams and materials characterization. See DOI: 10.1039/d2qi00156j

As the structural analogue of the famous Ni_2(dobdc) (Ni-MOF-74),[34] stable Ni_2(dobpdc),[35] Ni_2(olz)[36] and Ni_2(dotpdc)[37] possessed abundant OMSs after activation and honeycomb 1D channels with pore sizes 1.9, 2.2 and 2.6 nm, respectively, ranging from microporous to mesoporous pores (Fig. 1). These four MOFs provided an ideal platform for researching the effect of the pore size on D_2/H_2 separation. Based on the above considerations, we evaluated the D_2/H_2 separation of Ni_2(dobdc), Ni_2(dobpdc), Ni_2(olz) and Ni_2(dotpdc) frameworks by considering the effect of the pore size during the breakthrough process, which would propose optimal operating parameters for hydrogen isotope separation under simulated industrial conditions.

Results and discussion

The materials Ni_2(dobdc), Ni_2(dobpdc), Ni_2(olz), and Ni_2(dotpdc) were synthesized by the solvothermal method as previously reported.[32–35] Their purities were confirmed by PXRD patterns (Fig. S3–S6†). The involvement of Ni^{2+} and O atoms from the hydroxyl and carboxyl groups allowed these MOFs to retain their original skeletons under 180 °C and high vacuum, providing activated samples for gas sorption. N_2 sorption experiments further established the permanent porosities of these activated samples at 77 K, which showed the Brunner–Emmett–Teller surface areas (Fig. S2†) of 1280, 2574, 2659 and 2842 $m^2\ g^{-1}$ for the microporous Ni_2(dobdc) and Ni_2(dobpdc), and mesoporous Ni_2(olz) and Ni_2(dotpdc), respectively (Fig. 2). The pore size distributions of Ni_2(dobdc) (1.0 nm), Ni_2(dobpdc) (1.9 nm), Ni_2(olz) (2.2 nm) and Ni_2(dotpdc) (2.6 nm) frameworks were analyzed by the NLDFT method (Fig. S1†).

Upon activation and dehydration, a high concentration of OMS was exposed in the hexagonal channels of the material, which contributed to increased absorption at low pressures.[38–40] Due to its low zero-point energy and high enthalpy of adsorption, D_2 would be preferentially adsorbed onto OMSs,[41,42] while the large pore size allowed the diffusion process to proceed rapidly, thereby resulting in fast adsorption kinetics.[43,44]

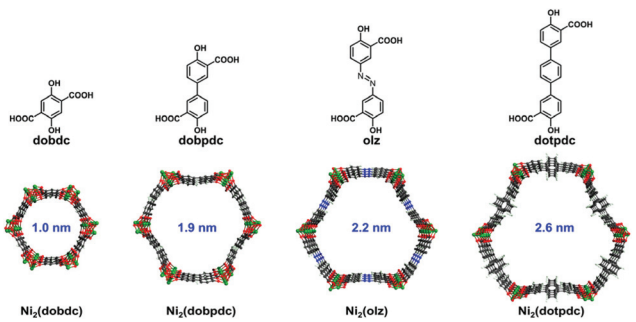

Fig. 1 Ligands and structures of Ni_2(dobdc), Ni_2(dobpdc), Ni_2(olz) and Ni_2(dotpdc) with different pore sizes.

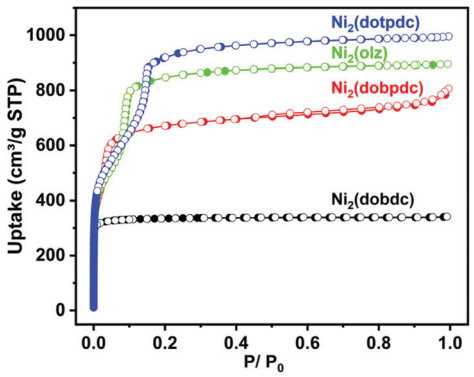

Fig. 2 N_2 sorption isotherms of Ni_2(dobdc), Ni_2(dobpdc), Ni_2(olz) and Ni_2(dotpdc) at 77 K (filled, adsorption; empty, desorption).

In order to better investigate the adsorption behaviour of this series of materials for hydrogen isotopes, adsorption isotherms were obtained for H_2 and D_2 at 77 K and 87 K, respectively. Ni_2(dobdc) exhibited uptakes of 11.2 mmol g^{-1} for H_2 and 11.6 mmol g^{-1} for D_2 at 110 kPa and 77 k, which were slightly higher than those of Ni_2(dobpdc) (H_2: 10.3 mmol g^{-1}, D_2: 11.3 mmol g^{-1}), Ni_2(olz) (H_2: 9.6 mmol g^{-1}, D_2: 10.6 mmol g^{-1}) and Ni_2(dotpdc) (H_2: 9.8 mmol g^{-1}, D_2: 10.83 mmol g^{-1}) (Fig. 3). It can be found that for the total adsorption, the microporous material had the highest adsorption of D_2 and H_2. However, at a very low pressure of 0.01 kPa, Ni_2(olz) exhibited the highest uptakes of D_2 (3.27 mmol g^{-1}) and H_2 (1.8 mmol g^{-1}), followed by Ni_2(dobpdc) (D_2: 3.15 mmol g^{-1}, H_2: 1.55 mmol g^{-1}), Ni_2(dobdc) (D_2: 2.7 mmol g^{-1}, H_2: 1.4 mmol g^{-1}) and Ni_2(dotpdc) (D_2: 2.25 mmol g^{-1}, H_2: 1.10 mmol g^{-1}) (Fig. 3 Insert). The higher adsorption can be attributed to the strong bonding between the OMSs and the hydrogen isotope molecules in the backbone, which was further confirmed by the enthalpy of adsorption calculated using the Clausius–Clapeyron equation (Table S1†). The D_2/H_2(50/50) selectivity of four MOFs was evaluated by the ideal adsorption solution theory (IAST) to predict their D_2/H_2 separation capacities (Fig. 4a and S7–S10†). It is found that the D_2/H_2(50/50) selectivity of Ni_2(olz) reached 5.6 under 77 K and 0.01 kPa, followed by Ni_2(dobpdc) (4.8), Ni_2(dobdc) (4.5) and Ni_2(dotpdc) (4.6). According to previous studies, Ni_2(olz) was by far the MOF with the highest IAST selectivity at 77 K.

Breakthrough experiments were carried out at 77 K to check the actual separation performances of Ni_2(dobdc), Ni_2(dobpdc), Ni_2(olz) and Ni_2(dotpdc). Therefore, the hydrogen isotope mixtures with different compositions, (H_2/D_2/Ne: 1/1/98), (H_2/D_2/Ne: 10/10/80) and (H_2/D_2: 50/50), were used to assess the practical D_2/H_2 separation capabilities of these isostructural materials. For these four adsorbents, when the (H_2/D_2/Ne: 1/1/98) mixture flowed through the packed column at a flow rate of 15 mL min^{-1}, H_2 always flowed out first because of its lower adsorption capacity and weaker bonding to the adsorbent, while D_2 remained in the packed column after the hydrogen separation. In packed columns filled with Ni_2(dobdc), the D_2 retention time reached a maximum of 240 min g^{-1}, longer

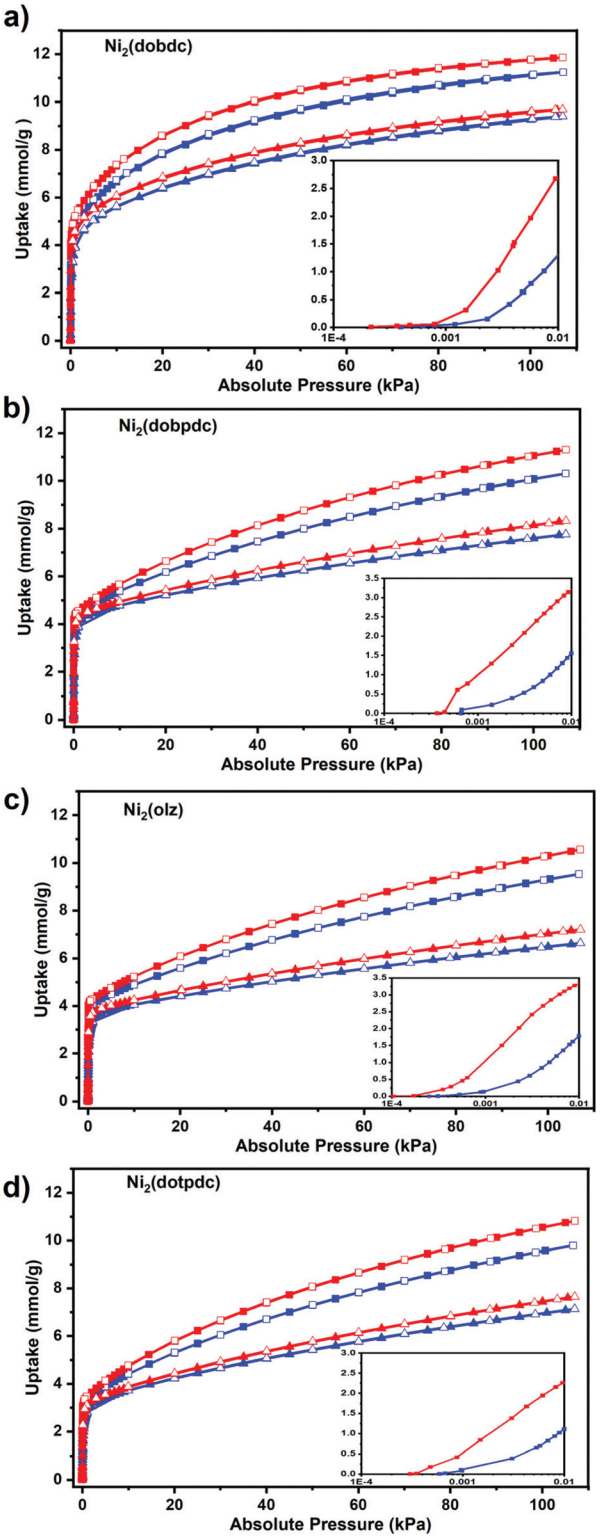

Fig. 3 The hydrogen isotope sorption of Ni_2(dobdc) (a), Ni_2(dobpdc) (b), Ni_2(olz) (c) and Ni_2(dotpdc) (d) at 77 and 78 K (filled, adsorption; empty, desorption). Insert: Sorption below a very low pressure of 0.01 kPa. Note: D_2 under 77 K (red □); H_2 under 77 K (blue □); D_2 under 87 K (red Δ); H_2 under 87 K (blue Δ).

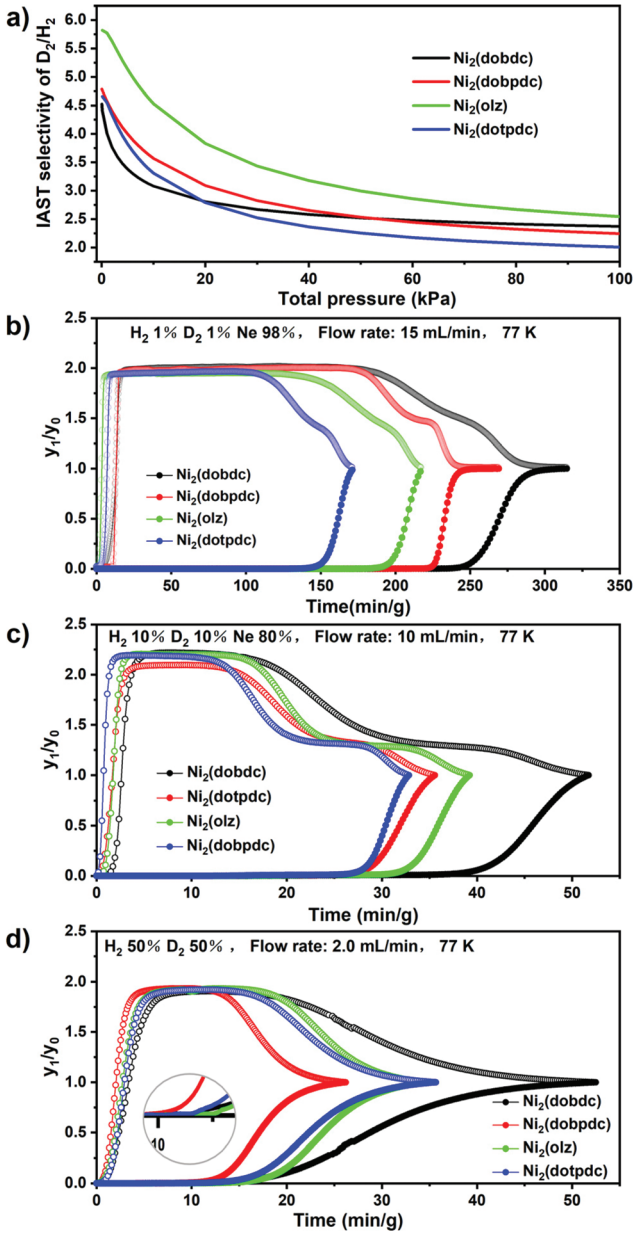

Fig. 4 (a) H_2/D_2(50/50) IAST selectivities of Ni_2(dobdc), Ni_2(dobpdc), Ni_2(olz) and Ni_2(dotpdc) at 77 K. (b–d) Breakthrough curves for D_2/H_2 separation on Ni_2(dobdc) (black), Ni_2(dobpdc) (red), Ni_2(olz) (green), Ni_2(dotpdc) (blue). The hollow circle represents H_2, and the solid circle represents D_2.

than those of Ni_2(dobpdc) (215 min g^{-1}), Ni_2(olz) (180 min g^{-1}) and Ni_2(dotpdc) (142 min g^{-1}) (Fig. 4b). D_2 retention times decreased with an increase in pore sizes of these four materials. When the gas mixture (H_2/D_2/Ne: 10/10/80) flowed through the packed column at a flow rate of 10 mL min^{-1}, the D_2 retention time of the microporous Ni_2(dobdc) reached a maximum of 36.4 min g^{-1}, but mesoporous Ni_2(olz) and Ni_2(dotpdc) exhibited D_2 retention times of 30.0 and 26.5 min g^{-1}, both of which exceeded that of microporous Ni_2(dobpdc) (25 min g^{-1}) (Fig. 4c). When a high concentration

of the hydrogen isotope mixture (H_2/D_2: 50/50) was passed through the packed column at a flow rate of 2 mL min^{-1}, mesoporous Ni_2(olz) showed the longest D_2 retention time of 15.0 min g^{-1}, which exceeded those of Ni_2(dobdc) (13.5 min g^{-1}) and Ni_2(dotpdc) (13.0 min g^{-1}) with the largest pore size. Microporous Ni_2(dobpdc) exhibited the shortest D_2 retention time of 10.0 min g^{-1} (Fig. 4d).

In the actual application of separation, excellent regeneration ability and structural stability were both important for suitable adsorbents; therefore, breakthrough experiments of the (H_2/D_2: 50/50) mixture on Ni_2(dobdc), Ni_2(dobpdc), Ni_2(olz) and Ni_2(dotpdc) were tested two times to evaluate their cycle performances. There is no noticeable degradation of the breakthrough time on these MOFs during their second cycling tests. Furthermore, the PXRD patterns confirm that the structural integrities of MOFs can be well preserved after the breakthrough tests (Fig. S3–S6†).

Compared to microporous Ni_2(dobdc) and Ni_2(dobpdc), the mesoporous Ni_2(olz) and Ni_2(dotpdc) always displayed lower D_2/H_2 separation capacities in a three-component mixture with low concentrations of D_2 and H_2. Simultaneously, they promoted their D_2/H_2 separation capacities to close or even surpass that of the famous Ni_2(dobdc) in the (H_2/D_2: 50/50) mixture. Such an interesting phenomenon was first observed in MOFs. In our opinion, in the absence of Ne gas during the breakthrough experiment, D_2 would be preferentially adsorbed onto the OMSs of the MOFs with large pores based on the CAQS effect because of their more accessible OMSs and migration rates ofthe hydrogen isotope. However, breakthrough experiments with Ne as the carrier gas might suffer competitive adsorption between Ne and hydrogen isotope. Heavier and larger Ne preferred to occupy accessible OMSs in MOFs with large pores rather than the unapproachable OMSs in MOFs with narrow pores, in which the reserved OMSs can preferentially adsorb D_2 to reach the D_2/H_2 separation. Further, a breakthrough experiment with Ne as the carrier gas would cause a new problem, the separation between Ne and D_2, leading to complicated separation procedures and high cost. Hence, the mesoporous isomers of MOF-74(Ni), particularly Ni_2(olz), might be ideal candidates for D_2/H_2 separation.

Conclusions

In summary, four analogues, including Ni_2(dobdc), Ni_2(dobpdc), Ni_2(olz) and Ni_2(dotpdc), possessed honeycomb 1D channels with abundant OMSs, enabling their D_2/H_2 separation capacities based on the CAQS effect. Two key factors, pore size and competitive adsorption between the hydrogen isotope and Ne as carrier gas, can significantly influence the MOF D_2/H_2 separation capacities during the ground-breaking experiments. In (H_2/D_2/Ne: 1/1/98) and (H_2/D_2/Ne: 10/10/80) mixtures, microporous Ni_2(dobdc) exhibited the best D_2/H_2 separation capacities with D_2 retention times of 240 and 36.4 min g^{-1}, respectively, as its narrow OMSs were inclined to adsorb small D_2 rather than bigger Ne during its competitive adsorption process. Nevertheless, it will cause a new problem of Ne/D_2 separation. In the (H_2/D_2: 50/50) mixture, mesoporous Ni_2(olz) exhibited the best D_2/H_2 separation capacity with a D_2 retention time of 15.0 min g^{-1} as its more accessible OMSs and migration rate of hydrogen isotope were inclined to adsorb heavier D_2 rather than H_2. These results supported the important guidance on choosing the MOFs for D_2/H_2 separation.

Experimental

Materials and general methods

All chemicals were obtained commercially and used as received without any further purification. Powder X-ray diffraction data were collected on a Rigaku Miniflex 600 diffractometer (Cu Kα λ = 1.540598 Å). Adsorption and desorption isotherms of all the gases under low pressure (0–1.1 bar) were measured using a Micromeritics ASAP 2020 PLUS instrument. The breakthrough experiments were performed using a home-built dynamic gas breakthrough setup.

Synthesis of Ni_2(dobdc)

The Ni_2(dobdc) sample was synthesized according to the reported method with minor modifications.[34] 2,5-Dihydroxyterephthalic acid (H_4dobdc) (40.42 mg, 0.204 mmol) was completely dissolved in a mixture of *N*,*N*-dimethylformamide, anhydrous ethanol and deionized water in a volume ratio of 15 : 1 : 1 after sonication, and then 198 mg (0.68 mmol) of $Ni(NO_3)_2{\cdot}6H_2O$ was added to the above mixture and stirred at room temperature to completely disperse in solution and to obtain a green synthetic solution. The solution was completely added to a stainless steel reactor with a PTFE liner, and the reaction was carried out at a temperature of 120 °C for 24 h. When the reaction was complete, the reactor was left to cool down naturally at room temperature. The product was collected once by centrifugation and further rinsed with DMF.

Synthesis of Ni_2(dobpdc)

Ni_2(dobpdc) sample was synthesized according to the reported method with minor modifications.[35] 2,5-Dihydroxybiphenyldicarboxylic acid (H_4dobpdc) (41.1 mg, 0.15 mmol) and $Ni(NO_3)_2{\cdot}6H_2O$ (109 mg, 0.375 mmol) were placed in the PTFE liner of a 20 ml reaction vessel. To this, 15 mL of mixed solvent (deionised water/DMF/anhydrous ethanol = 1 : 1 : 1) was added. The liner was covered and sonicated for 10 min and then placed in a stainless steel reactor. The reaction was carried out in an oven at 120 °C for 36 h. The samples were collected by filtration and rinsed with DMF.

Synthesis of Ni_2(olz)

Ni_2(olz) sample was synthesized according to the reported method with minor modifications.[36] The metal salt Ni $(NO_3)_2{\cdot}6H_2O$ (218 mg, 0.750 mmol) was dissolved in 10 mL of ethanol and 10 mL of H_2O, and olsalazine acid (H_4olz)

90.7 mg (0.300 mmol) was dissolved separately in 10 mL of *N*,*N*-diethylformamide (DEF). These solutions were combined and then distributed into three 20 mL glass scintillation vials, sealed with a PTFE-lined cap and heated in an oven at 120 °C for 24 h. The reaction mixtures were then combined, and the solvent was decanted. The orange solid was collected by filtration and washed with a continuous aliquot of DMF (3 × 20 mL).

Synthesis of Ni_2(dotpdc)

Ni_2(dotpdc) sample was synthesized according to the reported method with minor modifications.[37] 4,4″-Dihydroxy-[1,1′:4′,1″-terphenyl]-3,3″-dicarboxylic acid (H_4dotpdc) (147 mg, 0.75 mmol) and $Ni(NO_3)_2{\cdot}6H_2O$ (328 mg, 1.5 mmol) were placed in a 20 mL glass scintillation vial with 15 mL of mixed solvent (deionised water/DMF/anhydrous ethanol = 1 : 1 : 1) The vials were capped and sonicated until completely dissolved, and then heated in an oven at 100 °C for 24 h. The green crystal samples were collected by filtration and rinsed with DMF.

All of the above samples were, respectively, soaked in DMF for 3 days and then in methanol for 3 days, during which the solvent was changed every 12 h. The methanol-exchanged samples were heated at 180 °C for 24 h under dynamic vacuum (<10 μmHg) to remove the excess solvent, resulting in activated powder for gas sorption.

Breakthrough measurements

The breakthrough experiment was conducted with a custom-built dynamic gas breakthrough setup (Fig. S10†). The activated sample was first transferred to a glove box and loaded into a stainless-steel column (11 cm, inner diameter of 0.2 cm) with silica wool (30 mg) filling the void space. Then, the sorbent was heated at 120 °C for 10 h at a Ne flow rate of 10 mL min^{-1} to make the sample tight and fully activated. In order to ensure that the whole test process was carried out at 77 K, both the packed column and the pre-cooling line were cooled with liquid nitrogen for at least 30 min before the breakthrough measurements and continued to be cooled during the entire test. After cooling down of the temperature, the flow of Ne was then turned off, and the hydrogen isotope mixture was allowed to flow into the column. The composition and content of the outlet effluent were continuously monitored using a mass spectrometer (Pfeiffer Vacuum). For the different components of the gas used in the test, we used different flow rates to ensure that the test was performed under the best conditions. For (H_2/D_2/Ne: 1/1/98) a flow rate of 15 mL min^{-1} was used, for (H_2/D_2/Ne: 10/10/80) a flow rate of 10 mL min^{-1} was used and for (H_2/D_2: 50/50) a flow rate of 2 mL min^{-1} was used. After each breakthrough experiment, the sample was regenerated under Ne flow (10 mL min^{-1}) at 120 °C for 10 h.

Conflicts of interest

There are no conflicts to declare.

Acknowledgements

This work was financially supported by the Key Research Program of Frontier Sciences, by the CAS (QYZDB-SSW-SLH019), and by the National Natural Science Foundation of China (21771177).

Notes and references

1 C. Day and T. Giegerich, The Direct Internal Recycling concept to simplify the fuel cycle of a fusion power plant, *Fusion Eng. Des.*, 2013, **88**, 616–620.
2 R. Smith, D. A. J. Whittaker, B. Butler, A. Hollingsworth, R. E. Lawless, X. Lefebvre, S. A. Medley, A. I. Parracho, B. Wakeling and J.-E. Contributors, Hydrogen isotope separation for fusion power applications, *J. Alloys Compd.*, 2015, **645**, S51–S55.
3 M. Glugla, R. Lasser, L. Dorr, D. K. Murdoch, R. Haange and H. Yoshida, The inner deuterium/tritium fuel cycle of ITER, *Fusion Eng. Des.*, 2003, **69**, 39–43.
4 M. Glugla, D. K. Murdoch, A. Antipenkov, S. Beloglazov, I. Cristescu, I. R. Cristescu, C. Day, R. Laesser and A. Mack, ITER fuel cycle R&D: Consequences for the design, *Fusion Eng. Des.*, 2006, **81**, 733–744.
5 J. Y. Kim, H. Oh and H. R. Moon, Hydrogen Isotope Separation in Confined Nanospaces: Carbons, Zeolites, Metal-Organic Frameworks, and Covalent Organic Frameworks, *Adv. Mater.*, 2019, **31**, 23.
6 H. Oh and M. Hirscher, Quantum Sieving for Separation of Hydrogen Isotopes Using MOFs, *Eur. J. Inorg. Chem.*, 2016, **2016**, 4278–4289.
7 J. J. Cai, Y. L. Xing and X. B. Zhao, Quantum sieving: feasibility and challenges for the separation of hydrogen isotopes in nanoporous materials, *RSC Adv.*, 2012, **2**, 8579–8586.
8 D. W. Cao, H. L. Huang, Y. S. Lan, X. J. Chen, Q. Y. Yang, D. H. Liu, Y. Gong, C. J. Xiao, C. L. Zhong and S. M. Peng, Ultrahigh effective H2/D2 separation in an ultramicroporous metal-organic framework material through quantum sieving, *J. Mater. Chem. A*, 2018, **6**, 19954–19959.
9 S. A. FitzGerald, C. J. Pierce, J. L. C. Rowsell, E. D. Bloch and J. A. Mason, Highly Selective Quantum Sieving of D2 from H2 by a Metal–Organic Framework As Determined by Gas Manometry and Infrared Spectroscopy, *J. Am. Chem. Soc.*, 2013, **135**, 9458–9464.
10 J. E. Bachman, D. A. Reed, M. T. Kapelewski, G. Chachra, D. Jonnavittula, G. Radaelli and J. R. Long, Enabling alternative ethylene production through its selective adsorption in the metal-organic framework Mn2(m-dobdc), *Energy Environ. Sci.*, 2018, **11**, 2423–2431.
11 R. Yaris and J. R. Sams, Quantum Treatment of the Physical Adsorption of Isotopic Species, *J. Chem. Phys.*, 1962, **37**, 571–576.
12 K. Sumida, D. L. Rogow, J. A. Mason, T. M. McDonald, E. D. Bloch, Z. R. Herm, T.-H. Bae and J. R. Long, Carbon

Dioxide Capture in Metal–Organic Frameworks, *Chem. Rev.*, 2012, **112**, 724–781.
13 H. Furukawa, K. E. Cordova, M. O'Keeffe and O. M. Yaghi, ChemInform Abstract: The Chemistry and Applications of Metal-Organic Frameworks, *Science*, 2013, **341**, 1230444.
14 X.-M. Liu, L.-H. Xie and Y. Wu, Recent advances in the shaping of metal–organic frameworks, *Inorg. Chem. Front.*, 2020, **7**, 2840–2866.
15 X.-Y. Dao and W.-Y. Sun, Single- and mixed-metal–organic framework photocatalysts for carbon dioxide reduction, *Inorg. Chem. Front.*, 2021, **8**, 3178–3204.
16 Y. Cui, B. Li, H. He, W. Zhou, B. Chen and G. Qian, Metal–Organic Frameworks as Platforms for Functional Materials, *Acc. Chem. Res.*, 2016, **49**, 483–493.
17 Y. B. He, W. Zhou, G. D. Qian and B. L. Chen, Methane storage in metal-organic frameworks, *Chem. Soc. Rev.*, 2014, **43**, 5657–5678.
18 M. Tu, S. Wannapaiboon and R. A. Fischer, Liquid phase stepwise growth of surface mounted metal–organic frameworks for exploratory research and development of applications, *Inorg. Chem. Front.*, 2014, **1**, 442–463.
19 B. Liu, Y.-H. Jiang, Z.-S. Li, L. Hou and Y.-Y. Wang, Selective CO_2 adsorption in a microporous metal–organic framework with suitable pore sizes and open metal sites, *Inorg. Chem. Front.*, 2015, **2**, 550–557.
20 H. H. Wu, Q. H. Gong, D. H. Olson and J. Li, Commensurate Adsorption of Hydrocarbons and Alcohols in Microporous Metal Organic Frameworks, *Chem. Rev.*, 2012, **112**, 836–868.
21 Y. Peng, V. Krungleviciute, I. Eryazici, J. T. Hupp, O. K. Farha and T. Yildirim, Methane Storage in Metal–Organic Frameworks: Current Records, Surprise Findings, and Challenges, *J. Am. Chem. Soc.*, 2013, **135**, 11887–11894.
22 B. Li, H. L. Wang and B. L. Chen, Microporous Metal-Organic Frameworks for Gas Separation, *Chem. – Asian J.*, 2014, **9**, 1474–1498.
23 Z. J. Zhang, Z. Z. Yao, S. C. Xiang and B. L. Chen, Perspective of microporous metal-organic frameworks for CO_2 capture and separation, *Energy Environ. Sci.*, 2014, **7**, 2868–2899.
24 Z. R. Herm, E. D. Bloch and J. R. Long, Hydrocarbon Separations in Metal-Organic Frameworks, *Chem. Mater.*, 2014, **26**, 323–338.
25 Y. Wang, M. He, X. Gao, X. Wang, G. Xu, Z. Zhang and Y. He, A ligand conformation preorganization approach to construct a copper–hexacarboxylate framework with a novel topology for selective gas adsorption, *Inorg. Chem. Front.*, 2019, **6**, 263–270.
26 J. Ha, J. H. Lee and H. R. Moon, Alterations to secondary building units of metal–organic frameworks for the development of new functions, *Inorg. Chem. Front.*, 2020, **7**, 12–27.
27 P. Nugent, Y. Belmabkhout, S. D. Burd, A. J. Cairns, R. Luebke, K. Forrest, T. Pham, S. Q. Ma, B. Space, L. Wojtas, M. Eddaoudi and M. J. Zaworotko, Porous materials with optimal adsorption thermodynamics and kinetics for CO_2 separation, *Nature*, 2013, **495**, 80–84.
28 P. Kowalczyk, P. A. Gauden, A. P. Terzyk and S. Furmaniak, Impact of the carbon pore size and topology on the equilibrium quantum sieving of hydrogen isotopes at zero coverage and finite pressures, *J. Phys.: Condens. Matter*, 2009, **21**, 12.
29 I. Weinrauch, I. Savchenko, D. Denysenko, S. M. Souliou, H. H. Kim, M. Le Tacon, L. L. Daemen, Y. Cheng, A. Mavrandonakis, A. J. Ramirez-Cuesta, D. Volkmer, G. Schütz, M. Hirscher and T. Heine, Capture of heavy hydrogen isotopes in a metal-organic framework with active Cu(I) sites, *Nat. Commun.*, 2017, **8**, 14496.
30 S. A. FitzGerald, D. Mukasa, K. H. Rigdon, N. Zhang and B. R. Barnett, Hydrogen Isotope Separation within the Metal–Organic Framework Cu(I)-MFU-4 l, *J. Phys. Chem. C*, 2019, **123**, 30427–30433.
31 Y. Si, X. He, J. Jiang, Z. Duan, W. Wang and D. Yuan, Highly effective H2/D2 separation in a stable Cu-based metal-organic framework, *Nano Res.*, 2021, **14**, 518–525.
32 Y. Si, W. Wang, E.-S. M. El-Sayed and D. Yuan, Use of breakthrough experiment to evaluate the performance of hydrogen isotope separation for metal-organic frameworks M-MOF-74 (M=Co, Ni, Mg, Zn), *Sci. China: Chem.*, 2020, **63**, 881–889.
33 F. Wu, L. Li, Y. Tan, E.-S. M. El-Sayed and D. Yuan, The competitive and synergistic effect between adsorption enthalpy and capacity in D2/H2 separation of M2(m-dobdc) frameworks, *Chin. Chem. Lett.*, 2021, **32**, 3562–3565.
34 W. L. Queen, M. R. Hudson, E. D. Bloch, J. A. Mason, M. I. Gonzalez, J. S. Lee, D. Gygi, J. D. Howe, K. Lee, T. A. Darwish, M. James, V. K. Peterson, S. J. Teat, B. Smit, J. B. Neaton, J. R. Long and C. M. Brown, Comprehensive study of carbon dioxide adsorption in the metal–organic frameworks M2(dobdc) (M = Mg, Mn, Fe, Co, Ni, Cu, Zn), *Chem. Sci.*, 2014, **5**, 4569–4581.
35 T. M. McDonald, J. A. Mason, X. Q. Kong, E. D. Bloch, D. Gygi, A. Dani, V. Crocella, F. Giordanino, S. O. Odoh, W. S. Drisdell, B. Vlaisavljevich, A. L. Dzubak, R. Poloni, S. K. Schnell, N. Planas, K. Lee, T. Pascal, L. W. F. Wan, D. Prendergast, J. B. Neaton, B. Smit, J. B. Kortright, L. Gagliardi, S. Bordiga, J. A. Reimer and J. R. Long, Cooperative insertion of CO_2 in diamine-appended metal-organic frameworks, *Nature*, 2015, **519**, 303–308.
36 D. J. Levine, T. Runcevski, M. T. Kapelewski, B. K. Keitz, J. Oktawiec, D. A. Reed, J. A. Mason, H. Z. H. Jiang, K. A. Colwell, C. M. Legendre, S. A. FitzGerald and J. R. Long, Olsalaiine-Based Metal-Organic Frameworks as Biocompatible Platforms for H2 Adsorption and Drug Delivery, *J. Am. Chem. Soc.*, 2016, **138**, 10143–10150.
37 D. N. J. Xiao, J. Oktawiec, P. J. Milner and J. R. Long, Pore Environment Effects on Catalytic Cyclohexane Oxidation in Expanded Fe2(dobdc) Analogues, *J. Am. Chem. Soc.*, 2016, **138**, 14371–14379.
38 S. R. Caskey, A. G. Wong-Foy and A. J. Matzger, Dramatic Tuning of Carbon Dioxide Uptake via Metal Substitution in a Coordination Polymer with Cylindrical Pores, *J. Am. Chem. Soc.*, 2008, **130**, 10870–10871.

39 W. Zhou, H. Wu and T. Yildirim, Enhanced H2 Adsorption in Isostructural Metal–Organic Frameworks with Open Metal Sites: Strong Dependence of the Binding Strength on Metal Ions, *J. Am. Chem. Soc.*, 2008, **130**, 15268–15269.
40 E. D. Bloch, L. J. Murray, W. L. Queen, S. Chavan, S. N. Maximoff, J. P. Bigi, R. Krishna, V. K. Peterson, F. Grandjean, G. J. Long, B. Smit, S. Bordiga, C. M. Brown and J. R. Long, Selective Binding of O2 over N2 in a Redox–Active Metal–Organic Framework with Open Iron(II) Coordination Sites, *J. Am. Chem. Soc.*, 2011, **133**, 14814–14822.
41 J. Xu, R. Sinelnikov and Y. Huang, Capturing Guest Dynamics in Metal–Organic Framework CPO-27-M (M = Mg, Zn) by 2H Solid-State NMR Spectroscopy, *Langmuir*, 2016, **32**, 5468–5479.
42 H. Oh, I. Savchenko, A. Mavrandonakis, T. Heine and M. Hirscher, Highly Effective Hydrogen Isotope Separation in Nanoporous Metal-Organic Frameworks with Open Metal Sites: Direct Measurement and Theoretical Analysis, *ACS Nano*, 2014, **8**, 761–770.
43 D. Cattaneo, S. J. Warrender, M. J. Duncan, R. Castledine, N. Parkinson, I. Haley and R. E. Morris, Water based scale-up of CPO-27 synthesis for nitric oxide delivery, *Dalton Trans.*, 2016, **45**, 618–629.
44 A. L. Myers and J. M. Prausnitz, Thermodynamics of Mixed–Gas Adsorption, *AIChE J.*, 1965, **11**, 121–127.